# Effect of Overlap Rate on Temperature Field in Laser Cladding

**Xinyong Gong[a, *], Wei You[b], Mingyu Chen[c]**

School of Mechanical and Electrical Engineering, North China Institute of Science and Technology, Langfang 065201, China

[a]huagu1984@126.com, [b]429665519@qq.com, [c]1184755531@qq.com

*Corresponding author

**Keywords:** Laser Cladding; Numerical Simulation; Temperature Field; Overlap Rate

**Abstract:** A simple 3D model was used to simulate the process of laser cladding for the case of 316L stainless steel powder coating on the 45 steel. Effect of overlap rate on the temperature field was discussed using numerical simulation results. Isothermal contours for each substrate showed approximate ellipse shape, which distribution was changed significantly by adjustment of overlap rate. Furthermore, history of temperature load, such as peak temperature and thermal cycle was different for each substrate region, but all temperature amplitude was increased by the raise of overlap rate.

## 1. Introduction

Laser cladding was an advanced surface modification technology [1-3]. For large area coating, overlap between two adjacent laser scanning paths was inevitable due to restriction of laser spot (3~5 mm) [4, 5]. Overlap rate was defined as width ratio of coincidence region to a single cladding layer. By increasing overlap rate, surface roughness could be improved effectively [6], but re-melting and heat-affected zone for the successive laser scanning would become larger meanwhile. Temperature distribution of cladding parts would be changed obviously by overlap rate adjustment, by which evaluating indicators for the cladding quality such as microstructure, mechanical properties, residual stress distribution, were determined [7-9]. Overall temperature distribution for the physical model was hard to be measured only by experimental method, so a mathematical model was established in this paper, and temperature fields corresponding to 0, 1/3, 1/2 overlap rate were calculated by ANSYS software, which could be used as foundation for further theory and process research.

## 2. Model establishment

### 2.1 Physical Model

As shown in Fig.1, the present physical model was the laser cladding of 316L stainless steel powder on the surface of 45 steel substrate in raster long-path scanning mode, so scanning direction of the odd and even tracks was opposite. The plate was used to conduct the energy of the substrate. Another model information was summarized in Tab.1. Same process parameters (Tab.1) were adopted except the overlap rate. The overlapping area was two coating layers which was simplified as a rectangle shape in this model. To complete the same cladding area, number of cladding track and total time would be increased with overlap rate, which could be calculated as 5, 7, 9 and 75 s, 105 s, 135 s corresponding to the three overlap rates in Tab.1.

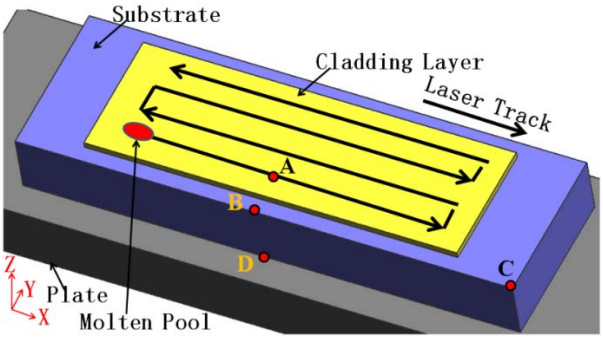


Figure 1. Physical model.

Table 1. Information Parameter of Physical Model.

| | Size (mm) | Material | |
|---|---|---|---|
| **Cladding Layer** | 60×20×0.5 | 316L Stainless Steel | |
| **Single Cladding Layer** | 60×4×0.5 | | |
| **Substrate** | 80×25×12 | 45 Steel | |
| **Process Parameter** | Laser Power *P*=1800 W, Scanning Speed *V*=4 mm/s | | |

### 2.2 Mathematical model

Initial temperature of the cladding layer, substrate, plate was all set as 20℃ in this model.

Reasonable boundary condition was necessary to solve the exact temperature field. Three kinds of boundary condition were involved as follows.

(1) In the region of laser beam, heat flux density was loaded on the surface of solid element subjected to laser irradiation, and the loading position (X, Y) was the function of cladding time (t). The partial differential equation of boundary condition was

$$-k\frac{\partial T}{\partial y}=\eta\frac{q}{\pi R^2},\quad \mathrm{R}\le \mathrm{R}_0 \tag{1}$$

In which, η, R0, k, q was laser absorption, radius of laser beam, thermal conductivity, laser power, respectively.

(2) Outside of the laser beam, heat convection existed between the cladding part and the air. The partial differential equation of the boundary condition was

$$-k\frac{\partial T}{\partial x_i}=h(T-T\mathrm{a})\qquad x_i=x,y,z,\quad \mathrm{R}\ge \mathrm{R}_0 \tag{2}$$

In which, ambient temperature Ta was 20 ℃, h was natural convection coefficient.

(3) On lower surface of the plate, a constant temperature was set as the plate was much larger than the cladding part. The partial differential equation of the boundary condition was

$$-k\frac{\partial T}{\partial y}=T_c \tag{3}$$

In which, Tc was the constant temperature, and 20 ℃ was selected in this model.

## 3. Results and Discussion

Temperature distribution at the end of laser cladding process, under the condition of 0, 1/3, 1/2 overlap rate, were shown in Fig.2, respectively. The physical domain above 1399~1435℃ can be regarded as molten pool, which is the melting temperature for the cladding layer (316L stainless steel). A 4×4 mm rectangular laser spot was set in this model. The molten pool along X direction was slightly larger than 4 mm, so all powders injected could be melted and remelting occurred in the local area of the previous cladding layer. However, width of the molten pool along with the laser

scanning direction was less than 4 mm, which was due to inadequate heating of cladding powder in the laser spot front and the energy loss to the cladding substrate. The above shape characteristics of the molten pool could be fully consistent with the experimental observations.

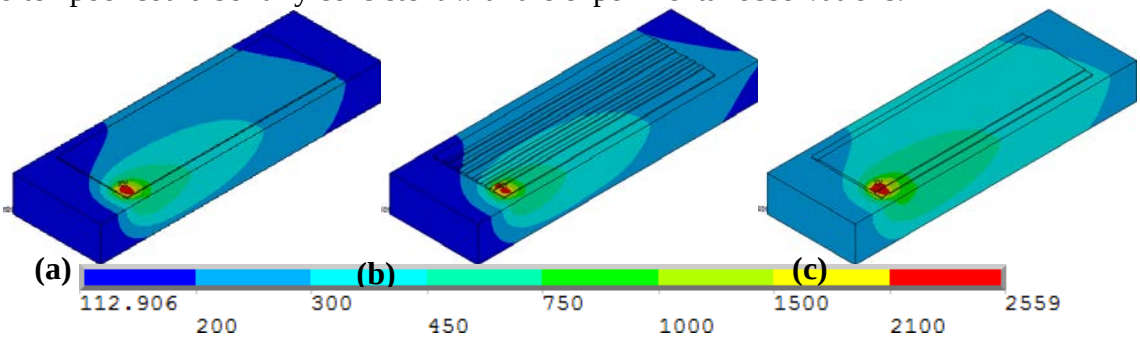


Figure 2. Temperature distribution at the end of laser cladding (a) 0 overlap rate, (b) 1/3 overlap rate, (c) 1/2 overlap rate.

Temperature distribution of substrate surface at the end of laser cladding was shown in Fig.3. The local position above 1493~1530℃ would experience the melting and solidification process, which is the melting point of the substrate (45# steel). The metallurgical bonding between the cladding layer and the substrate could be realized by the above three overlap rates conditions, so process parameters selected were proved. Isothermal contours of above three substrates in X-Z and Y-Z planes showed oval shape approximately, and their long axes were consistent with laser scanning direction, but distinction lay in position and range of each contour.

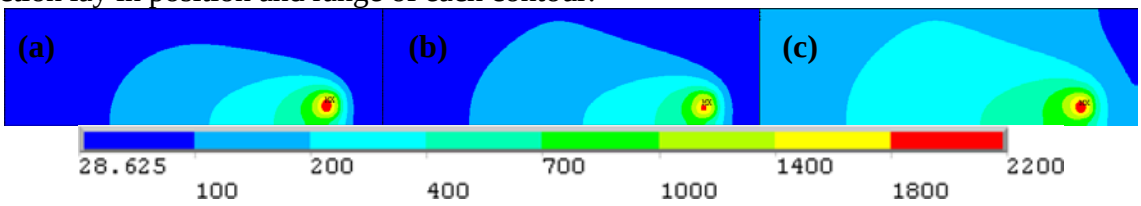


Figure 3. Temperature on the surface of substrate(a) 0 overlap rate, (b) 1/3 overlap rate, (c) 1/2 overlap rate.

To proceed further theoretical analysis of the transient temperature field in laser cladding process, 4 positions of the physical model are taken as key points of A, B, C, D in Fig1. The A, B, D, (C) points were located at the midpoint (endpoint) of each ridge in X-direction. Transient temperature curves of each key point in 0 overlap rate condition were show in Fig.4(a), in which curve A, B, (C, D) corresponded to the left (right) side of the vertical axis, due to relatively low temperature of point C, D. Scanning time of single track was 15s, so total time for this cladding model of 0 overlap rate was 75s (15s×5 tracks). Time of peak temperature in each cycle of temperature fluctuation for the key point depended on its physical domain coordinates. As the laser beam scanned to the midpoint of each cladding track (7.5 s+15n, n=0, 1, 2, 3, 4), time of peak temperature for point A and B were (8.01 s, 23.26 s, 39.76 s, 56.76 s), (8.01 s, 24.01 s, 40.76 s, 58.01 s) respectively, and there was little difference only increased slightly with the number of scanning track. However, first peak temperature for point C, D appeared at 19.26 s, 11.01 s, which were far away from the molten pool relatively. Above delay time of point D was about 3.5 s, which would increase further with the laser cladding process. Different from A, B, D, endpoint C experienced heating and cooling process twice only, and one thermal cycle lasted 30 s, so temperature load of different regions varied greatly in the model. In addition, valley temperature in each thermal cycle would be increased with the cladding process, so omitting the effect of sharp heating in local area of the substrate caused by laser radiation, the whole substrate was in the process of energy storage.

Temperature variation curves for position B in 0, 1/3, 1/2 overlap rate condition were shown in Fig.4(b). For the same cladding size, number of laser scanning track would be increased with the overlap rate, so processing time of the above three models were 75 s, 105 s, 135 s, respectively. Temperature histories in the first 75 s for these three curves were the same exactly, which trended to

be gentle with time. But difference existed in fluctuation range for each temperature curve. Peak and valley temperature in 1/2 overlap rate condition was relatively high, which meant thermal storage would be increased with overlap rate.

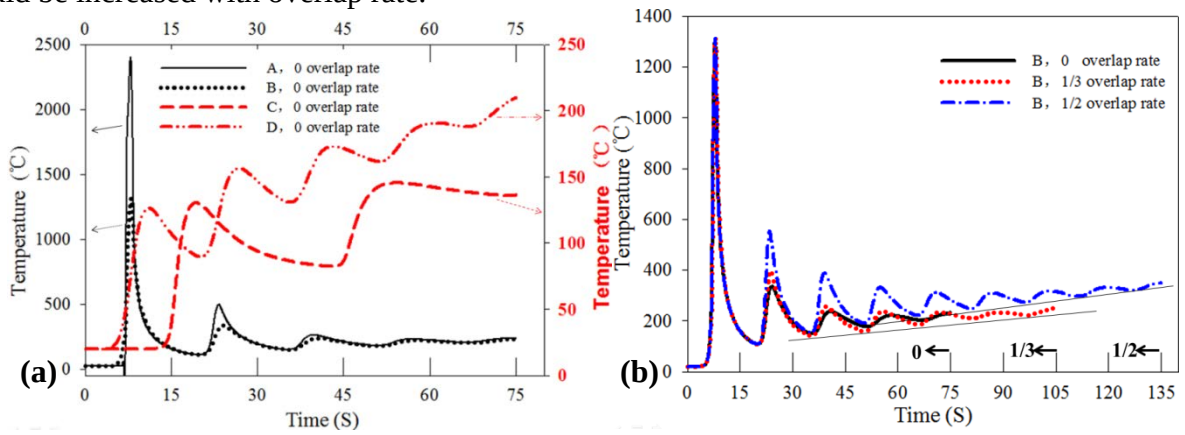


Figure 4. Transient temperature of critical point (a) Point A, B, C, D for 0 overlap rate (b) Point B for different overlap rate.

## 4. Conclusion

Laser cladding with different overlap rate were simulated by ANSYS software, then the temperature field was solved and analyzed. The main conclusions are as follows.

(1) Isothermal in the cladding substrate presented ellipse shape, and its long axis was consistent with the laser scanning direction, which would be affected significantly by adjustment of the overlap rate.

(2) Laser radiation is the main cause for the formation of the molten pool, which temperature distribution would be affected indirectly by the overlap rate through the change of substrate temperature.

(3) Different temperature loads applied to each position of the cladding substrate, including peak temperature and thermal cycle. Overall heat storage of the substrate would be increased with the overlap rate.


## Acknowledgments

This work was financially supported by Langfang Science and Technology Research and Development Program (No.2017011035), Basic Scientific Research Service Fee of Central University (No.3142015012, No.3142015097) and Innovation, Entrepreneurship Training Program for College Students (No. 201811104021).


## References


[1] Z. C. Liu, Q. H. Jiang, T. Li, S. Y. Dong, S. X. Yan, H. C. Zhang, and B. S. Xu, Journal of Cleaner Production **133,** 1027-1033 (2016).

[2] P. R. Zhang, and Z. Q. Liu, The International Journal of Advanced Manufacturing Technology **82,** 1707 (2016).

[3] J. H. Yao, V. S. Kovalenko, Q. L. Zhang, A. Mykola, X. D. Hu, and W. F. Wang, Surface Engineering and Applied Electrochemistry **46,** 266 (2010).

[4] J. Brandenburg, V. Neu, H. Wendrock, B. Holzapfel, H. U. Krebs, and S. Fahler, Applied Physics A **79,** 1005 (2004).

[5] W. M. Steen, Laser Surface Treatment of Metal **12,** 369 (1986).

[6] S. Y. Xian, A. P. Yang, Y. Yan, P. Yue, and P. Zhang, Aerospace Manufacturing Technology **2,** 26 (2011).

[7] W. P. Dai, C. Y. Tang, M. W. Wang, J. M. Kang, X. D. Chen, and X. Zhang, Hot Working Technology **10,** 178 (2016).

[8] M. Z. Xi, Y. Z. Zhang, P. Z. Zhang, L. K. Shi, and J. Cheng, Chinese Journal of Laser **11,** 1045 (2002).

[9] L. K. Shi, S. Y. Gao, M. Z. Xi, H. Z. Ji, Y. Z. Zhang, and B. L. Du, Acta Metallurgica Sinica **5,** 459 (2006)